Cloud Publications
International Journal of Advanced Remote Sensing and GIS
2015, Volume 4, Issue 1, pp. 1092-1108, Article ID Tech-422
ISSN 2320 - 0243

Research Article **Open Access**

GIS-Based Estimation of Potential Solar Energy on Flat Roofs in Maadi, Cairo, using True Ortho World View Image and Digital Surface Model

Lamyaa Gamal El-deen Taha[1] and Hala Adel Effat[2]

[1]Division of Aviation and Aerial Photography, National Authority for Remote Sensing and Space Sciences, NARSS, Cairo, Egypt
[2]Division of Environmental Studies and Land Use, National Authority for Remote Sensing and Space Sciences, NARSS, Cairo, Egypt

Correspondence should be addressed to Hala Adel Effat, haeffat@yahoo.com, lamyaa@narss.sci.eg

Publication Date: 30 June 2015

Article Link: http://technical.cloud-journals.com/index.php/IJARSG/article/view/Tech-422

Abstract This research is concerned with the use of remotely sensed data in the estimation of the solar energy potentiality of the flat roofs in El Maadi District, Cairo. A solar radiation model was applied using a digital surface model (DSM) generated from two Worldview stereo satellite images using the digital photogrammetric workstation (Leica Photogrammetric Suite) LPS. The procedures included applying orientation with Rational Polynomial Coefficients (RPC) with and without GCPs, tie point measurements, aerial triangulation, automatic DSM and editing, true ortho-rectification. The accuracy of the DSM has been assessed and reported for both methods. The ortho-rectification, of stereo satellite images has been performed. A PAN true ortho-images with 0.5 m resolution resulted from applying orientation with rational polynomial coefficients (RPCs) refined with four accurate differential ground control points (DGCPs) and a high accurate DSM derived from stereo images were generated. Two classification methods were conducted (SVM and ANN) on the true ortho-image. First method without utilizing texture, the second utilizing texture features of Grey Level Co-occurrence Matrix (GLCM) as inputs. The SVM of the ortho-image and texture features overall accuracy was 93.4%, kappa coefficient was 0.92 and ANN of ortho-image and texture features overall accuracy of 91.2% and kappa coefficient was 0.90. Using the generated DSM as input, the area solar radiation model in ESRI ArcGIS was run. The model resulted in an annual total radiation grid for year 2015 which was converted to average daily radiation in kilowatt hour/square meters per day. A sample of 265 buildings footprints was extracted from the classification and used for the estimation. Assuming that 50% roof areas are available for solar Photovoltaic (PV), 12% PV grid conversion efficiency and 0.6 performance ratio and using ESRI zonal statistics tool, the technical potentiality for solar PV electricity generation for the sample buildings was calculated, classified into five classes and mapped.
Keywords *Worldview Stereo; True Ortho-Images; DSM Generation; Geo-Positional Accuracy; Solar Radiation; Photovoltaic; Rooftop PV Systems*

1. Introduction

Solar energy is one of the more promising sustainable energy sources due to its accessibility. Over recent years, the technology that uses the PV (photovoltaic) effect for the production of electrical power has progressed immensely (Lukac et al., 2014). Private investors as well as local authorities have a rising interest in identifying roof areas which are suitable for mounting solar systems (Kassner et al., 2008). As some buildings' roofs are more suitable than others, regarding the received solar irradiance, the solar potential (average daily or total received irradiance on a given surface (Lukac et al., 2014) presents an important issue in urban planning and the environmental health of modern sustainable cities.

1.1. Literature Review

Many of the studies to estimate potential generation from PV systems through estimating rooftop area have been developed. Such studies ranged from simple multipliers of total building space to methods that employ complex geographic information systems (GIS) or three-dimensional (3-D) models. Constant-value, manual selection, and GIS-based methods are the three main methods that are commonly used (Meluis et al., 2013).

Many of the constant-value methods of rooftop-area estimation consider typical rooftop configurations and estimate a multiplier that can be applied to an entire region. A variation of the constant-value method involves estimating available rooftop space based on the population density of a region (Ladner-Garcia and O'Neill-Carrillo, 2009; Vardimon, 2011). The buildings are classified by type (commercial, industrial, residential) and size, and a constant value of 30% is applied to the entire building stock as an assumed availability factor for rooftop area Vardimon, 2011. Reports from NREL (Eiffert, 2003) and the International Energy Agency (IEA, 2001) estimate rooftop availability for all 23 IEA countries. Each country is assigned a constant rooftop-availability value based on population density, which factors in each of the other components. Eiffert (2003) derived a value that describes the suitability of rooftops relative to total ground floor area.

Manually selecting methods derive rooftops from sources such as aerial photography. Johnson and Armanino (2004) in Marin, California while Armanino and Johnson (undated) conducted a study in Phoenix, Arizona to estimate rooftop suitability; in both studies, rooftops are manually identified from aerial imagery based on their solar resource, land use, and location away from large objects that could create large shadows. The footprints for these buildings are digitized and their rooftop areas are calculated. The total area is reduced by 25% to account for loss of PV performance. Wittmann and Bajons (1997) and Nguyen and Pearce (2012, 2013) selected rooftops from aerial imagery with characteristics that appear suitable for rooftop PV (e.g., flat and south-facing roofs). Nguyen and Pearce (2012, 2013) apply constant values to the selected rooftops, ranging from 50% to 62.5% for pitched roofs and 100% for flat roofs. Zhang et al. (2009) use Google Earth to identify suitable rooftops. Their study selects only roofs with south-, southeast-, and southwest-facing planes to select suitable rooftops. Rooftops are also visually inspected for shading and building obstructions. Anderson et al. (2010) use IMBY web application to estimate the suitable rooftop area for a sample of buildings in New York City,

In GIS-based methods, the majority of rooftop analyses use GIS-based methods for estimating the suitable space for rooftop PV. Ideal values for rooftop characteristics are input into a computer model, and the GIS software determines areas of high suitability. GIS-based methods use primarily 3-D models to determine solar resource or shadow effects on buildings. The 3-D models are most often generated from orthophotography and light detection and ranging (LiDAR) data, and they are combined with slope, orientation, and building structure data to estimate total solar energy generation potential. Nguyen and Pearce (2013) analysts ran a sample of 100 buildings in Ontario through the

GRASS r.sun tool. Rooftops with a southeast- through southwest-facing aspect (90 to 270 degrees) and a slope within 15 degrees of the local latitude are considered suitable for PV. Compagnon (2004) conducted an analysis in Fribourg, Switzerland that uses a 3-D building model for 61 buildings in the study area. The building model is run through RADIANCE/DAYSIM, and researchers place a minimum of 1,000 kilowatt-hours per square meter (kWh/m^2) on the model to determine suitable rooftop areas. Rooftop area is considered to be suitable for PV if it has a slope less than or equal to 60 degrees and a solar resource value of at least 609 kWh/m^2. Tooke et al. (2011) use the ArcGIS Solar Analyst tool to model the solar resource available on rooftops. The study concludes that solar radiation on rooftops varies from hourly and seasonally, and that trees reduce solar radiation on rooftops by an average of 38%. Another study to use the proportion of flat roofs versus pitched roofs is an analysis for San Diego (Anders and Bialek undated). All building footprints greater than 3,000 square feet were digitized and are run through ArcGIS Solar Analyst to determine the total solar resource available for large-area buildings. Rooftop area is manually assigned to one of three classifications: 20% suitable area, 60% suitable area, or 80% suitable area. Once total rooftop area is estimated, the area is reduced by 20% to account for shading.

A study of Lisbon, Portugal (Santos et al., 2011), uses LiDAR data to create a DSM that is then used as an input in the ArcGIS Area Solar Radiation tool to create a solar surface map. A solar radiation map is created for each month of the year, and the 12 values for each pixel are averaged to determine a final solar radiation value. Rooftop areas are considered suitable for PV if at least 10 contiguous square meters have more than 1.68 megawatt-hours per square meter (MWh/m2) of solar radiation and have a slope of less than 45 degrees. Latif et al. (2012) use LiDAR data to create a DSM for Georgetown, Malaysia. From this DSM, slope, aspect, and solar radiation are calculated. The thresholds for slope include one scenario with a 15-degree maximum slope and a second scenario with a 30-degree maximum slope. Only rooftops with south-, southwest-, or southeast-facing aspects are considered. Additionally, rooftops identified as suitable for PV are required to have at least 1,000 watts per square meter and be at least 2.6 square meters in size, accounting for a 1.5 square meter PV panel size as well as 15% buffer space for the mounting frame and panel spacing.

The solar tools in ESRI ArcGIS can be used to analyze the effects of the sun over a specific geographic location over a range of time intervals. The solar radiation analysis tools in ESRI ArcGIS 10, calculates insolation across a landscape or for specific locations, based on methods from the hemispherical viewshed algorithm developed by Rich et al. (1994) and further developed by Fu and Rich (2000, 2002). The total amount of radiation calculated for a particular location or area is given as global radiation. The calculation of direct, diffuse and global insolation was repeated for each feature location or every location on the topographic surface, producing insolation maps for an entire geographic area. The Solar Analysis tools in ArcGIS 10.2 allows for one to take into account how the daily and seasonal shifts of the sun angle, elevation, orientation (slope and aspect), and shadows from surrounding features affect the amount of solar radiation received on any particular surface (in Wh/m^2) (ESRI, 2012). In order to perform the analysis, an input 2D raster representation (DEM) of the case study area was created as discussed in the previous section. This model was imported into ArcMap 10.2, and the Area Solar Radiation tool was used to model the incoming solar radiation on the case study area. Area Solar Radiation is an extension of the Spatial Analyst tool in ESRI ArcGIS. It is capable of performing calculations on complex rooftop shapes, as it takes topographic constraints from the model into account (Chow et al., 2014). The Area Solar Radiation tool calculates the amount of insolation received across an entire landscape at a specific location based on the hemispherical view shed algorithm. The hemispherical view shed approach is used to assess sky obstructions for any location on or above a topographic surface. It allows for the performance of rapid calculations and permits users the control over the level of resolution to use in the simulations (Rich et al., 1994). The view shed method is used together with sun position and sky direction information for the calculation of direct, diffuse and total solar radiation for each specified location to calculate an accurate solar insolation map. The main input parameters of the Area Solar Radiation tool are: latitude, sky size resolution, day and hour intervals, time configuration, z-factor, slope/aspect, calculation directions, zenith and azimuth divisions, diffuse radiation model, diffuse proportion, and transitivity (ESRI, 2012).

2. Location of the Study Area

Maadi is an affluent district in the south of Cairo the capital of Egypt. It lies to the south on the river Nile about 12 km upstream from downtown Cairo, on the east bank. Maadi is the least densely populated district in Greater Cairo. The oldest area is El Sarayat, composed mostly of villas and low-rise buildings and is one of the most affluent parts of Maadi along with the adjacent Degla area. There are several high-rises along the Corniche by the River, as well as the newer, eastern part, known as Degla which is chosen for this application (Beattie, 2005).

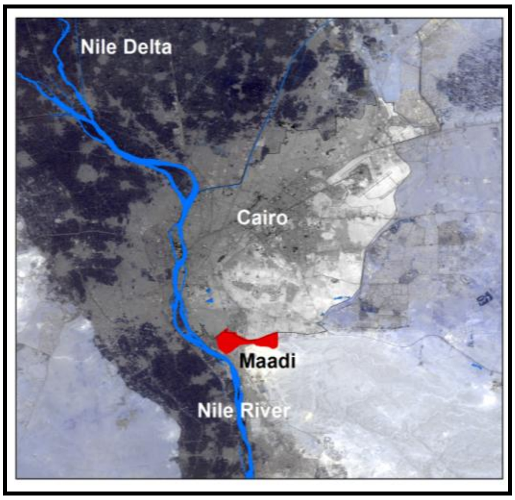

Figure 1: *Location of the Study Area*

3. Description of the Data Set

The following data Sources were available

- A 1:50 000 topographic maps
- Two Stereo pan Worldview images Worldview Dated 2013 and RPC files
- DGPS Ground control points and check points obtained with 10 cm accuracy in X, Y, Z.

4. Methodology

Solar modeling functions in GIS require data that is spatially referenced with detailed elevation information in raster data format (digital elevation model or digital surface model). There are two types of digital elevation models, digital terrain model (DTM) and digital surface model (DSM). DTMs represent the bare ground surface excluding any man-made features while DSMs represent the earth's surface including all objects on it.

4.1. Creating the DSM from World View Stereo Satellite Images

Two world-View stereo satellite images (four images) were available for the present study. The production of DSM have been performed on the digital photogrammetric workstation (Leica Photogrammetric Suite) LPS. The digital photogrammetric procedures include orientation with RPC approach collection of GCPs, tie point measurements, aerial triangulation, automatic DSM creation and DEM editing.

The first goal was to derive true ortho-images and digital surface models (DSM) from the worldview stereo data by applying the Rational Polynomial Coefficients (RPC) Model for the orientation process with direct geo-referencing and without ground control points (GCPs). The second goal was to derive true ortho-images and digital surface models (DSM) from the worldview stereo data by applying the Rational Polynomial Coefficients(RPC) Model for the orientation process with ground control points (GCPs), As a first step, the interior and exterior orientation of the sensor, delivered as ancillary data from positioning and attitude systems were extracted. A dense image matching for producing DSM, Additionally, true ortho-images were generated from the images. In a second step few GCPs (4) were used to improve the direct geo-referencing process. This method improved the absolute accuracy of the resulting true ortho-images and DSM significantly.

The quality of the generated DTM has been validated. After that orthorectification of the two world-View stereo satellite images have been performed on the digital photogrammetric workstation LPS. The following section describes the procedure 1.

4.1.1. Photogrammetric Project Creation

A project was created to include Worldview images, the datum were chosen WGS84 and the projection UTM ZONE 36. The software Leica Photogrammetric Suite (LPS) Module of Erdas Imagine 2013 software was utilized for the processing of the stereoscopic images. The image was imported to the project.

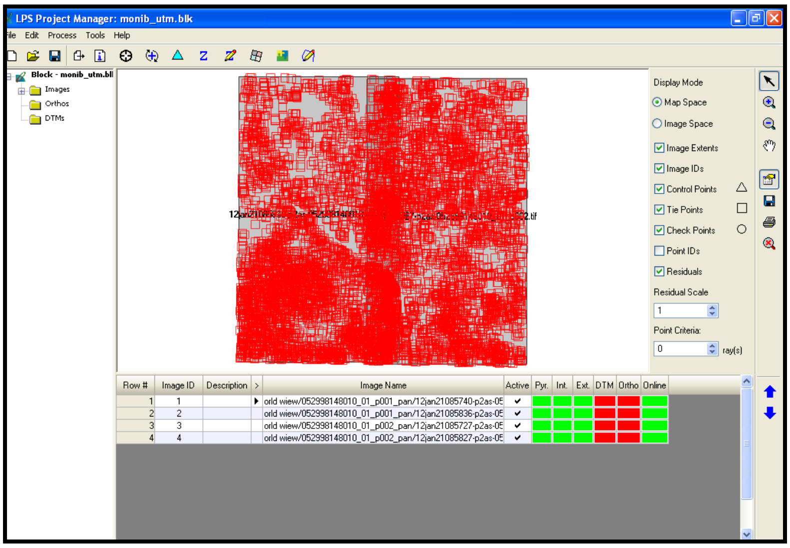

Figure 2: *Project Creation in Leica Photogrammetric Suite*

Figure 3: *World View Stereo Pair Imageries*

4.1.2. Rational Polynomial Coefficients (RPC) Model

The rational function model is the ratio of two polynomials and is derived from the physical sensor model and on-board sensor orientation. The rational polynomials coefficients (RPCs) are supplied with the WorldView imagery (Zhang and Fraser, 2008). They are expressing the relation between the image and the ground coordinates and are based on the direct sensor orientation of the satellite (Buyuksalih et al., 2008). Because RPCs are derived from orientation data originating from the satellite ephemeris and star tracker observations, without reference to ground control points (GCPs), they can give rise to geo-positioning biases. These biases can be accounted for by introducing additional parameters. After the bias compensation process, bias-corrected RPCs can be generated by incorporating bias compensation parameters into the original RPCs, allowing bias-free application of RPC positioning without the need to refer to additional correction terms (Zhang and Fraser, 2008).

- Using RPC + Automatic tie points generation (for image orientation)
- Using Collected GCPs (Improvements by few GCPs) + Automatic tie points (for image orientation)

4.1.3. Interior Orientation and Triangulation

Interior orientation is not required with Worldview images. The software read it from the header file.

4.1.4. DSM Generation Using Image Matching

DEMs can be produced by automatic DEM extraction from stereoscopic satellite images collected by WorldView-1 and WorldView-2 satellites. In general ground control points are recommended to improve the image geo-location accuracy (Poli and Caravaggi, 2012). The orientation has been simplified by using rational polynomial functions and the direct sensor orientation has been improved, allowing, in some cases, the image processing and DSM generation without ground control information (Poli and Caravaggi, 2012). Automatic Point Measurement (APM) includes automatic assistance of ground control point measurement, automatic tie point collection and automatic tie point transfer from one image to another. The DSM was then generated using image matching.

4.1.5. Assessment of DSM Quality Using Check Points (Vertical Accuracy)

The procedure for assessing digital elevation model (DEM) or DSM quality involves examination of the vertical accuracy and completeness. In general ground control points are recommended to improve the image geo-location accuracy In general ground control points are recommended to improve the image geo-location accuracy (Poli and Caravaggi, 2012; Aguilar et al., 2013; Zhang and Fraser, 2008). DSM vertical accuracy could be attained by computing height differences between independently surveyed check points and planimetrically corresponding DSM points. Independent check points (ICPs) should be at least three times more accurate than the expected accuracy to be verified and the minimum required sample size to assure a reliable accuracy assessment is not easy to specify (Aguilar et al., 2013). Thirty independent check points were used for DSM evaluation. The results indicated the RMS of 6.8m was achieved using RPC only. The results indicated the RMS of 5m was achieved using RPC bias compensated.

4.1.6 Ortho-rectification of Stereo Images Using Digital Photogrammetric Workstation

The images are ortho-rectified using the DSMs with a pixel size 0.5m and nearest neighbor resampling. The thirty independent DGPS check points were used for DSM evaluation resulted in RMS in X = 0.66 RMS in Y= 0.49 RMST= 0.82 using RPC only and RMS in X =0.49.RMS in Y= 0.43 RMST=0.65 using RPC bias compensated.

The ortho-rectified image resulted from RPC bias compensated was used.

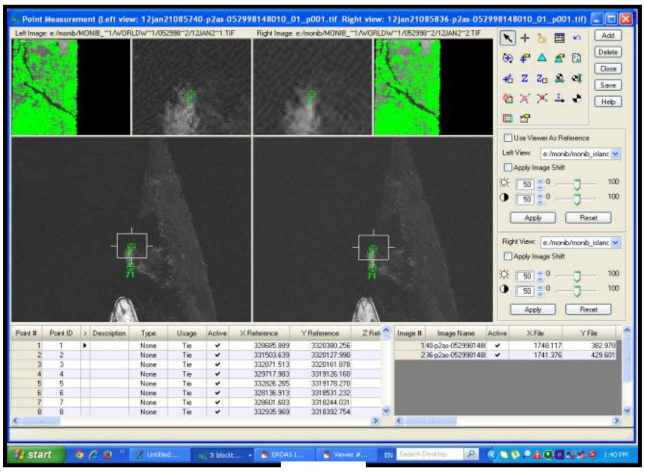

(a)

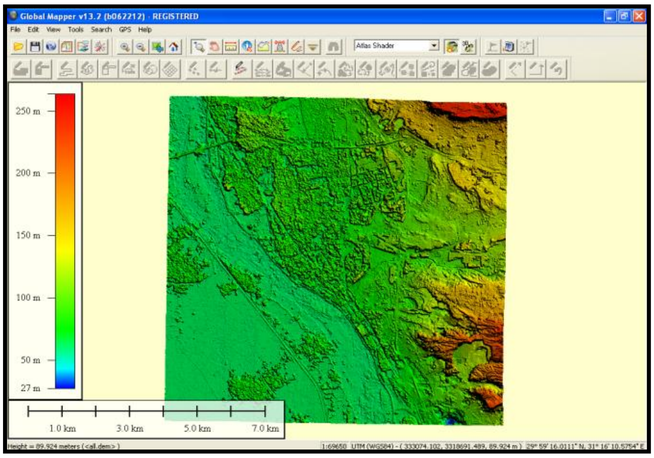

(b)

Figure 4: *(a) A Snapshot of Image Matching Process (b) A Snapshot of the Extracted DSM in Global Mapper*

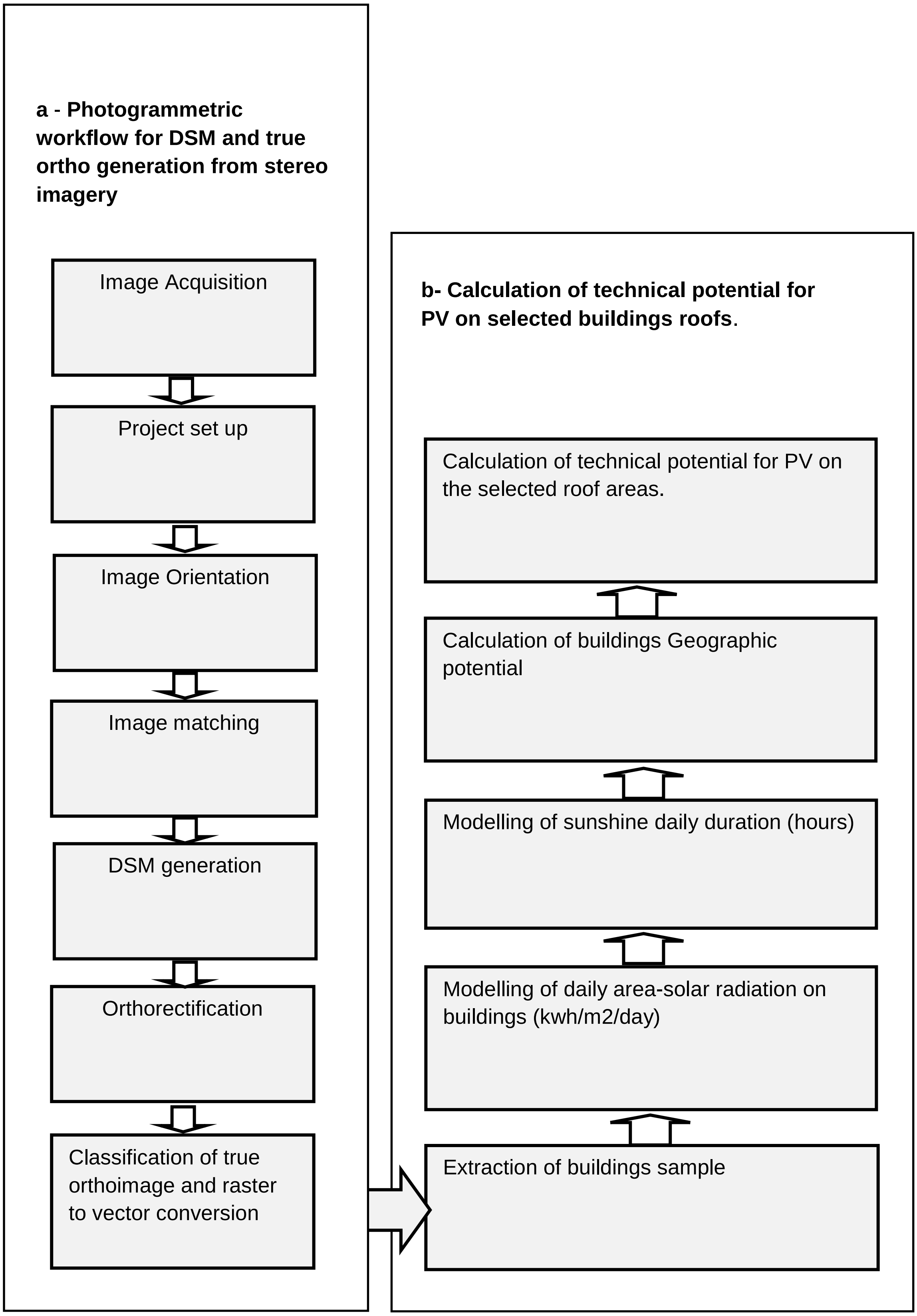

Figure 5: *Work Flow for the Applied Methodology*

4.2. Estimation of the Solar Energy on the Roof Buildings

4.2.1. Extraction of a Sample of Buildings

The study area was limited to El-Maadi neighborhood in order to select a sample set of buildings. Two methods were experimented for extraction of Buildings:

First, Traditional digitizing: A traditional on-screen digitizing process was adopted to isolate the 265 buildings footprints from the World View corrected satellite imagery using the digitizing tools in ESRI Arc map, this step was done for reference and for editing the classification results of the panchromatic imagery.

The panchromatic imagery has a limitation in the classification results as differentiation of ground features with higher complexities probably due to high interclass spectral confusion as well as the absence of multispectral information. However, studies found that accurate discrimination between land use/cover classes depends not only on spectral information but also on spatial (textural) information of the high resolution image. Therefore, the potential of the high resolution panchromatic data and the necessity of spatial information (texture) (Kamiran and Sarker, 2014) are to be considered. Therefore, for automatic building extraction, two classification methods (support vector machine (SVM) and artificial neural network (ANN) with and without utilizing from texture were experimented. In the Texture Extraction step: mean and variance extracted by gray level co-occurrence matrix (GLCM) are used to describe the textural features. Signatures were collected for five classes to represent the land use/land cover of the study area: buildings, roads, vegetation, shadows and desert. Thirty signatures have been collected in each class then signatures evaluation was carried out to ensure that they represent unique land covers and that they will produce the most accurate classification. The collected signatures were evaluated, and the result is accepted before the classification process.

The accuracy assessment demonstrates that SVM achieved overall accuracy 84.32% and kappa coefficient 0.81 using true orthoimage and SVM achieved overall accuracy 93.41% and kappa coefficient 0.92 using true orthoimage and texture features. ANN achieved overall accuracy 82.12% and kappa coefficient 0.78 using true orthoimage and ANN achieved overall accuracy 91.21% and kappa coefficient 0.90 using true orthoimage and texture features. When textural features are introduced as the input of the classifiers, both the overall and class accuracies are enhanced.

After that buildings were separated in a mask from SVM classification of true orthoimage and texture features then morphological operations were used Morphological opening with kernel size of 3×3 followed by morphological closing with kernel size of 3×3 have been applied to the resulted building mask using ENVI 4.8 software. Then raster to vector conversion was performed for resulted on 265 buildings and manually edited using the previously digitized buildings footprints. The buildings were assigned an ID numbering and imported into a geographic database. The buildings footprints were later used for the Estimation of the Solar Energy on the Roof Buildings.

4.2.2. ArcGIS AreaSolar Radiation Module

The ArcGIS AreaSolar Radiation tool computes the global solar radiation on a surface for any time of day for each month of the year, investigating in every direction whether there are any obstacles, natural and artificial, and cross referencing this information with the map of the sun and the sky map. The calculation is based on the position of the sun and calculates direct beam radiation; while the second is based on the atmosphere and calculates diffuse solar radiation. Reflected solar radiation is excluded from the calculation (Minghetti et al., 2011; Africani et al., 2013). The latitude for the site area (units: decimal degree, positive for the north hemisphere and negative for the south hemisphere) is used in calculations such as solar declination and solar position (ESRI ArcGIS Area solar radiation tool)

The annual solar radiation falling on the roofs of the selected buildings sample was modeled. Using ESRI Areasolar radiation module, the annual solar radiation grid in Wh/m2/year and the solar duration in hours were derived. The buildings footprints layer was used to extract the radiation values from the area solar radiation grid. The solar irradiation received on each building rooftop can be identified using the Area solar grid and the footprints which were extracted from the classification of the true orthoimage and converted to vector as explained in an earlier step (section 4.2.1).

4.2.3. Calculation of the Solar Photovoltaic Potentials for the Roofs

To calculate the solar photovoltaic potentials for the roofs, the area solar grid was converted from watt hour per square meters/year (wh/m2/year) to kilowatt hour/square meters per day (kwh/m2/day).

According to Hoogwijk (2004) and Mahtta (2014) the technical potential (E*i*) of solar PV electricity generation in a grid cell *i* is given by equations 1 and 2 as follows:

$$G_i = A_i \times h^{-1} \times I \qquad (1)$$

Where, G*i* is the geographical potential as shown in equation (2)
I is the insolation in kwh/m2/day,
$\boldsymbol{A_i}$ is the suitable area for PV installation,
h is the number of sunshine hours in a day,

$$Ei = Gi \times \eta m \times pr \qquad (2)$$

E_i is the technical potential of solar photovoltaic system.
η*m* is the conversion efficiency for PV modules which depends on type of PV cells and module temperature.
$\mathbf{p}_r$ is the performance ratio of the PV system

The $\mathbf{p}_r$ is defined as the ratio of on-field performance of the system to its performance in standard test condition of 1000 W/m^2 global insolation, 25°C module temperature and 1.5 air mass (Ramachandra et al., 2011). It takes into account the overall effect of losses on the output of the system. Losses can be due to inverter inefficiency, direct current (DC) to alternate current (AC) conversion, soiling or snow and incomplete use of irradiance by reflector system. Mostly available PV systems have **p*r*** in between 0.66 and 0.85 (Turkenberg, 2004). Mahtta (2013) used a conversion efficiency of 12% and performance ratio of 0.6 in a study for photovoltaic power plants in New Delhi. Assuming a similarity of environmental and economic conditions in Cairo, the same ratios were adopted in this study.

The area solar radiation tool in ESRI ArcGIS produced the areasolar radiation grid in watt hours per square meters for the year 2015. The grid was converted to kilowatt hours per square meters per day. ***I*** (Figure 7-b). A further optional output of the model is the solar duration map for the same period. The duration grid was divided by the number of days in the year to produce the average annual daily sunshine hours in the studied year **(*h)*** (Figure 8-b). To identify the suitable roofs for PV installation, the buildings layer was used as a mask to extract the values from the area solar grid in kwh/m2/day. This produced the roof area solar grid which was classified into five classes based on the radiation values. The roof areas were calculated in a new field which was created in the attribute table for the potential areas (A_i), assuming 50% of such roof areas are suitable.

The technical potential PV estimated energy for the suitable roofs was calculated using the *zonal statistics as table* tool. Using the suitable-roof-areas layer, the values from the area solar radiation grid kwh/m^2 were extracted in a zonal statistics table (*I*). Same step was repeated to extract the values from the solar duration grid (in hours) (*h*). Using a table join function, the geographic potential G*i* was calculated for each building. A 12% conversion efficiency and 0.6 performance ratio (after Mahtta, 2013) were used to calculate the technical potential for solar PV electricity generation for each of the 265 buildings.

5. Results and Discussion

A DSM and true orthoimages have been produced from the worldview stereo data using the digital photogrammetric workstation (Leica Photogrammetric Suite) LPS. It was found that the resulted true orthoimages and digital surface models (DSM) from the worldview stereo data by applying the Rational Polynomial Coefficients (RPC) Model with ground control points (GCPs) is better accuracy than the resulted true orthoimages and digital surface models (DSM) from the worldview stereo data by applying the Rational Polynomial Coefficients (RPC) Model with direct georeferencing and without ground control points (GCPs).

Thirty independent check points were used for DSM evaluation. The results indicated the RMS of 6.8m was achieved using RPC only and RMS of 5m was achieved using RPC bias compensated. The Thirty independent DGPS check points for true ortho evaluation resulted in RMS in X =0.66.RMS in Y= 0.49 RMST=0.82 using RPC only and RMS in X =0.49.RMS in Y= 0.43 RMST=0.65 using RPC bias compensated.

By visual inspection, in urban areas the road network, building blocks can be clearly recognized from the result of the ortho-rectified image (Figure 6)

Figure 6: *Subset of Orthoimage Produced Using Worldview Stereo Satellite Images*

Two methods were experimented for extraction of Buildings. First, Traditional digitizing: A traditional on-screen digitizing process was adopted to isolate the roofs footprints for 265 buildings from the World View geometrically corrected satellite imagery using the digitizing tools in ESRI Arc map. Second, Automatic building extraction was conducted: using two classification methods (SVM and ANN) with and without utilizing from texture. In the Texture Extraction step, two textures features (mean and variance) extracted by gray level co-occurrence matrix (GLCM). The accuracy assessment demonstrates that SVM achieved overall accuracy 84.32% and kappa coefficient 0.81 using true orthoimage and SVM achieved overall accuracy 93.41% and kappa coefficient 0.92 using orthoimage and texture features.

ANN achieved overall accuracy 82.12% and kappa coefficient 0.78 using true orthoimage and ANN achieved overall accuracy 91.21% and kappa coefficient 0.90 using true orthoimage and texture features. When textural features are introduced as the input of the classifiers, both the overall and class accuracies are enhanced. It was found also that automatic building extraction gave more satisfactory results compared to manual. The buildings were separated in a mask from SVM classification of orthoimage and texture features. Morphological operations were used morphological opening with kernel size of 3×3 followed by morphological closing with kernel size of 3×3 have been applied to the resulted building mask using ENVI 4.8 software.

The building footprints, the digital surface model (DSM) and the areasolar radiation grid for the study area are shown in Figures 7a, 7b and 7c respectively. Figures 8a, 8b depict the areasolar radiation and the number of sunshine hours falling on the roofs respectively. The potential areas for PV installations (A*i*) calculated by multiplying the roof areas (A*i)* by 50% accounting for other roof usage. The buildings solar duration in hours per day (h) and the solar radiation in kwh/m2 were used to apply equation (1) to calculate the geographic potentiality G*i* for the buildings. The technical potential E*i* for the solar photovoltaic of the investigated buildings was derived using equation (2) is shown in Figure 9.

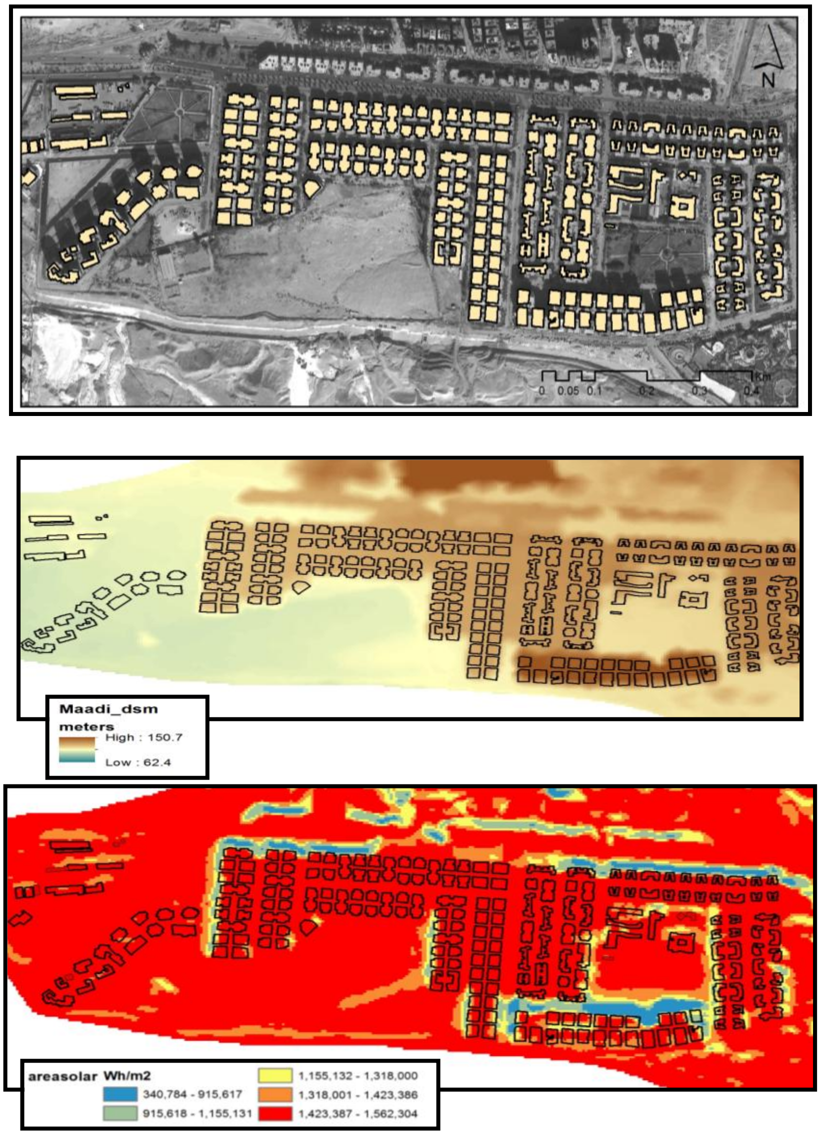

Figure 7: *A) Extracted Buildings Overlayed with the Ortho-Image. B) Digital Surface Model C) Areasolar Radiation Map Derived from the Digital Surface Model*

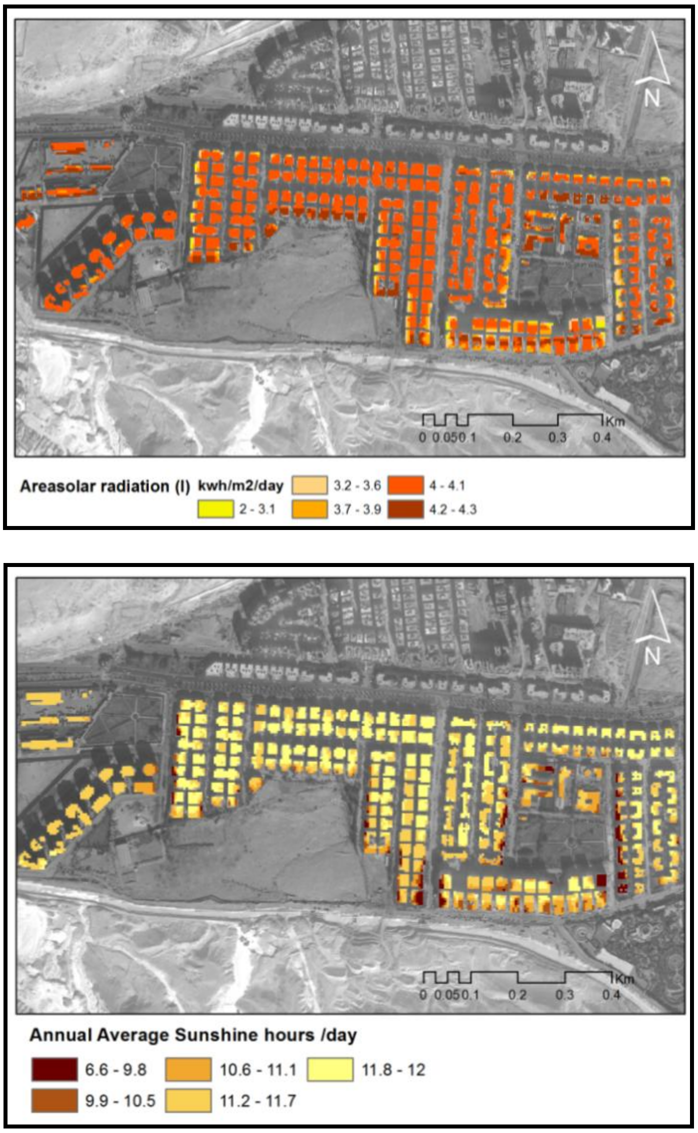

Figure 8: *A) Areasolar Radiation Map. B) Annual Average Sunshine Hours Falling on the Roofs Par Day*

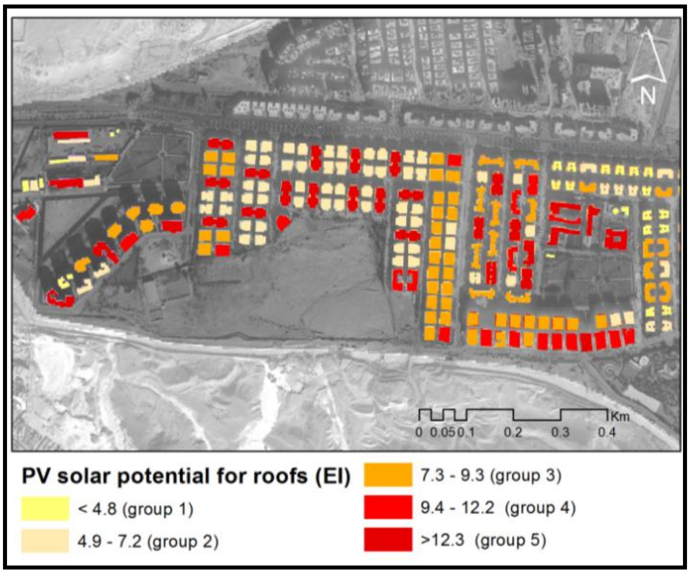

Figure 9: *Solar PV Potentiality Map for the Five Classes of Roofs*

Examination of the building roofs for solar PV grid potential (Figure 9) revealed that: there was a variation in the range of values in the five classes ranging between 0.5 to more than 12.9. Such variation is probably due to the variation in roof areas, daily radiation falling on each roof. Statistics for the values of the five classes are shown in Figure 10 and Table 1.

To understand the impact of the shadow, which is a result of the building morphology and the site topography, further analysis is needed, yet it is not in the scope of the current study. Except for few buildings, the effect of building heights and trees were quite limited. The reason is that most of the buildings are multi-story and exceed the heights of the trees. It was noticed that the larger the roof area, the more potentiality for solar PV. Therefore, it can be deduced that the multi-story buildings (buildings growing vertically with less roof areas) are not ideal for fulfilling the building needs for PV potential energy. Second factor is the building orientation; buildings oriented south, southwest and southeast have highest PV potentiality, providing that no shadows obstruct the direct radiation. It was noticed that the urban morphology and spatial distribution is a third factor. Buildings overlooking an open area (bare land, wide streets fell in a higher category for PV potentiality having no shadow from neighboring buildings. It was noticed that buildings in close proximity to each other have to maintain the same heights to avoid shadow effects from higher to lower buildings).

Table 1: *Statistics for the Buildings PV Technical Potentiality Classes*

PV Potentiality	Count	Minimum	Maximum	Mean	Standard Deviation	Percentage
Class 1	30	0.5	4.8	3.4	1.1	13
Class 2	80	5.1	7.2	6.2	0.5	36
Class 3	61	7.4	9.3	8.3	0.5	27
Class 4	21	9.4	12.2	10.5	0.9	9
Class 5	33	12.6	24.7	14.1	2.1	15

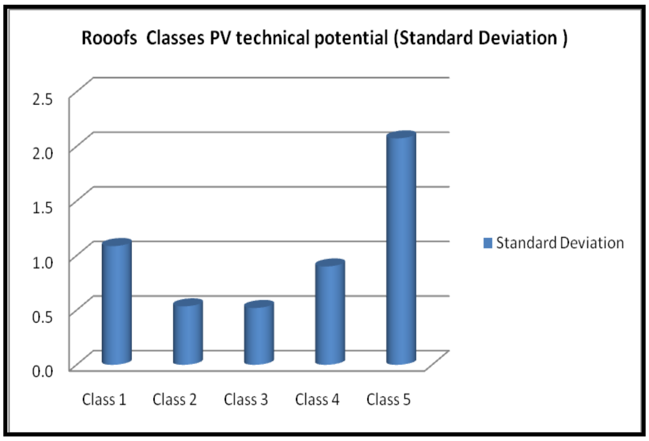

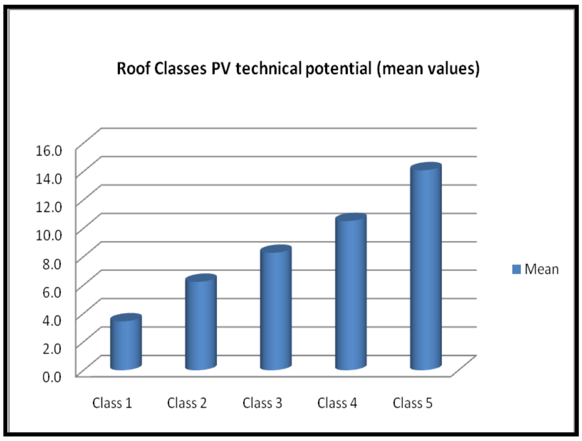

Figure 10: *Statistics for the Five Potential Roof Buildings Classes for Solar PV*

6. Conclusions

In this research stereo worldview images were used for true ortho-image generation, for image classification and the generation of digital surface model (DSM). The same data were used to extract the buildings roofs. The DSM was used to model the solar radiation and to assess the roof potentials for solar photovoltaic cells. Experiments were carried out for automated extraction of a digital surface model (DSM) and true ortho-image from HRS data of World view satellite in digital photogrammetric workstation LPS module. It was concluded that:

- The analysis conducted in Erdas Imagine 2013 and based only on the Metadata provided by the sensor (RPC) with and without ground control points (GCPs). It was found that applying (RPC) with GCPs for orientation produces better accuracies for (DSM) and true ortho-image.

- Automatic building extraction was conducted: using two classification methods (SVM and ANN) with and without utilizing from texture. In the Texture Extraction step, two textures features (mean and variance) extracted by gray level co-occurrence matrix (GLCM). The accuracy assessment demonstrates that SVM achieved overall accuracy 84.32% and kappa coefficient 0.81 using true ortho-image and SVM achieved overall accuracy 93.41% and kappa coefficient 0.92 using ortho-image and texture features.

- Areasolar radiation model was used to calculate the global radiation (direct and indirect) considering the sun duration in hours. It was possible to calculate the geographic potentiality of the area and eventually the solar PV potentiality for the buildings' roofs from the digital surface model derived from the Worldview imageries.

- The roof solar PV technical potentiality E_i is derived from the geographic potentiality. It ranged between 3.4 to 14.1 mean values. Variation is caused by several factors, for the present study the spatial distribution of the average solar radiation, roof areas and average daily sun hours were studied.

Acknowledgement

The authors acknowledge the National Authority for Remote Sensing and Space Sciences, NARSS for providing the data for this work. The editing and comments of the reviewers of this research paper is gratefully appreciated.

References

Africani, P., Lamberini, A., Minghetti, A. and Pselli, E., 2013: *Integration of LIDAR into a Municipal GIS to Study Solar Radiation.* International Archives of the Photogrammetry, Remote Sensing and Spatial Information Sciences, Volume XL-1/W1, ISPRS Hannover Workshop 2013, 21-24 May 2013, Hannover, Germany.

Aguilar, M.A., Saldana, M.M., and Aguilar, F.J. *GeoEye-1 and WorldView-2 Pan- Sharpened Imagery for Object-Based Classification in Urban Environments.* International Journal of Remote Sensing. 2013. 34 (7) 10, 2583-2606.

Anders, S. and Bialek, T. (undated). *Technical Potential for Rooftop Photovoltaics in the San Diego Region. Energy Policy Initiatives Center* - University of San Diego School of Law and San Diego Gas & Electric.

Anderson, K.H., Coddington, M.H. and Kroposki, B.D., 2010: *Assessing Technical Potential for City PV Deployment using NREL's In My Backyard Tool.* Prepared for 35th IEEE Photovoltaic Specialists Conference. Honolulu, Hawaii.

Armanino, D. and Johnson, G. (undated). *Phoenix/Scottsdale Solar Rooftop Capacity.* County of Marin Community Planning Department.

Buyuksalih, G., Baz, I., Bayburt, S., Jacobsen, K. and Alkan, M., 2008: *Geometric and Mapping Potential of Worldview-1 Images.* ISPRS Hannover Workshop 2009. High Resolution Earth Imaging for Geospatial Information. Accessed 1 May 2015 at http://www.ipi.uni-hannover.de/322.html

Chow, A., Fung, A.S. and Li, S. *GIS Modeling of Solar Neighborhood Potential at a Fine Spatiotemporal Resolution.* Buildings. 2014. 4; 195-206.
Beattie, A., 2005: *Cairo, a Cultural History*. Oxford University Press Inc., New York.

Compagnon, R. *Solar and Daylight Availability in the Urban Fabric*. Energy and Buildings. 2004.

Eiffert, P., 2003: *Non-Technical Barriers to the Commercialization of PV Power Systems in the Built Environment*. NREL/TP-550-31976. Golden, CO: National Renewable Energy Laboratory.

ESRI. ArcGIS Help 10.1. 2012: *Understanding Solar Radiation Analysis.* Available online: http://resources.arcgis.com/en/help/main/10.1/index.html#//009z000000t8000000.

Fu, P. and Rich, P.M., 2000: *The Solar Analyst 1.0 Manual*. Helios Environmental Modeling Institute (HEMI), USA.

Fu, P. and Rich, P.M. *A Geometric Solar Radiation Model with Applications in Agriculture and Forestry*. Computers and Electronics in Agriculture. 2002. 37; 25-35.

Hoogwijk, M., 2004: *On the Global and Regional Potential of Renewable Energy Sources.* Utrecht University. http://www.library.uu.nl/digiarchief/dip/diss/2004-0309-123617/full.pdf.

Johnson, G. and Armanino, D. Solar 2004: Conference: *GIS Tools for Community Development Applications.* San Rafael, CA: County of Marin Community Development Agency.

Kamiran, N. and Sarker, M.L.R., 2014. *Exploring the Potential of High Resolution Remote Sensing Data for Mapping Vegetation and the Age Groups of Oil Palm Plantation 8th.* International Symposium of the Digital Earth (ISDE8), IOP Publishing.

Kassner, R., Koppe, W., Schüttenberg, T. and Bareth, G. *Analysis of the Solar Potential of Roofs by using Official LIDAR Data*. The International Archives of the Photogrammetry, Remote Sensing and Spatial Information Sciences. 2008. 37 (4) Beijing.

Ladner-Garcia, H.P. and O'Neill-Carrillo, E. *Determining Realistic Photovoltaic Generation Targets in an Isolated Power System. Prepared for 2009.* IEEE Power & Energy Society General Meeting, July 26-30, 2009. Calgary, Alberta Canada.

Latif, Z.A., Zaki, N.A.M. and Salleh, S.A., 2012: *GIS-based Estimation of Rooftop Solar Photovoltaic Potential using LiDAR.* Prepared for the 2012 IEEE 8th International Colloquium on Signal Processing and its Applications, March 23-25, 2012. Melaka, Malaysia.

Luk, A.C.N., Seme, S.D., Zlaus Stumberger, G. and Zalik, B. *Buildings Roofs Photovoltaic Potential Assessment Based on LiDAR (Light Detection and Ranging) Data.* Energy. 2014. 66; 598-609.

Mahtta, R., Joshi, P.K. and Jindal, A.K. *Solar Power Potential Mapping in India Using Remote Sensing Inputs and Environmental Parameters*. Renewable Energy. 2014. 71; 255-262.

Melius, J.R., Margolis, R. and Ong, S. National Renewable Energy Laboratory. 2013: *Estimating Rootop Suitability for PV: A Review of Methods, Patents and Validation Techniques*. (Accessed March 14, 2015) at www.nrel.gov/publications.

Minghetti, A., Africani, P. and Paselli, E., 2011: *Bologna Solar City, A Web Application for the Analysis of Potential Energy: From Estimating Solar Radiation to the Realization of the Application.* Proceedings 17th International Conference Building Services, Mechanical and Building Industry Days Urban Energy Conference, Debrecen, 13-14 October 2011. 25-30.

Nguyen, H.T. and Pearce, J.M. *Incorporating Shading Losses in Solar Photovoltaic Potential Assessment at the Municipal Scale*. Solar Energy. 2012. 86; 1245-1260.

Nguyen, H.T. and Pearce, J.M. *Automated Quantification of Solar Photovoltaic Potential in Cities.* International Review for Spatial Planning and Sustainable Development. 2013. 1 (1) 57-70.

Poli, D.I and Carvaggi, I. *Digital Surface Modeling and 3D Information Extraction from Space Borne Very High Resolution Stereo Pairs European Commission.* Joint Research Centre Institute for the Protection and Security of the Citizen.

Ramachandra, T.V., Jian, R. and Krishnadas, G. *Hotspots of Solar Potential in India.* Renewable Sustainable Energy Review. 2011. 15 (6) 3178-3186.

Rich, P.M., Dubayah, R., Hetrick, W.A. and Saving, S.C., 1994: *Using Viewshed Models to Calculate Intercepted Solar Radiation: Applications in Ecology.* American Society for Photogrammetry and Remote Sensing Technical Papers. 524–529.

Santos, T., Gomes, N., Brito, M., Breire, S., Fonseca, A. and Antonio, J. 2011: *Solar Potential Analysis in Lisbon using LiDAR data.* Prepared for the 31st EARSeL Symposium and 35th General Assembly, May 30-June 2, 2011. Prague, Czech Republic.

Tooke, T.R., Coops, N.C., Voogt, J.A. and Meitner, M.J. *Tree Structure Influences on Rooftop-Received Solar Radiation*. Landscape and Urban Planning. 2011. 102; 73-81.

Turkenberg W.C., 2004: *Renewable Energy Technologies.* Goldemberg J. editor. World Energy Assessment. Washington D.C., UNDP: 2004. 220-272.

Vardimon, R. *Assessment of the Potential for Distributed Photovoltaic Electricity Production in Israel*. Renewable Energy. 2011. 36; 591-594.

Wittmann, H. and Bajons, P. *Identification of Roof Areas Suited for Solar Energy Conversion Systems.* Renewable Energy. 1997. 11 (1) 25-36.

Zhang, C. and Fraser, C. *Generation of Digital Surface Model for High Resolution Satellite Imagery*. The International Archives of the Photogrammetry, Remote Sensing and Spatial Information Sciences. 2008. 37. Part B1. Beijing.

Zhang, X., Walker, R., Salisbury, M., Hromiko, R. and Schreiber, J. *Creating a Solar City: 2009: Determining the Potential of Solar Rooftop Systems in the City of Newark*. University of Delaware, Center for Energy and Environmental Policy.